Dalton Transactions

Accepted Manuscript

ROYAL SOCIETY OF CHEMISTRY

www.rsc.org/dalton

Dalton Transactions

Cite this: DOI: 10.1039/c0xx00000x

www.rsc.org/xxxxxx

ARTICLE TYPE

Synthesis of magnetic ion-imprinted composite and its selective separation and preconcentration of U(VI)

Mancheng Liu, Changlun Chen*, Tao Wen, Xiangke Wang

Received (in XXX, XXX) Xth XXXXXXXXX 200X, Accepted Xth XXXXXXXXX 200X

DOI: 10.1039/b000000x

The U(VI) magnetic ion-imprinted composite (MIIC) with a uniform core–shell structure for the selective separation and preconcentration of U(VI) was prepared by copolymerization of a ternary complex of uranyl ions with 4-vinylpyridine (4-VP) and acrylamide in the presence of 2,2′-azobisisobutyronitrile. The sorption of U(VI) on the MIIC from aqueous solution was evaluated. The maximum sorption capacity of MIIC for U(VI) was 354.85 $mg \cdot g^{-1}$, which was much higher than that of magnetic nonimprinted composite. The MIIC could be recovered by desorbing the U(VI)-loaded MIIC with 0.5 $mol \cdot L^{-1}$ HNO_3, and the surface morphology of MIIC after five consecutive sorption/desorption cycles was significantly damaged. The competitive sorption experiments showed that the MIIC had a desirable selectivity for U(VI) over a range of competing metal ions. The MIIC may be a promising sorbent material for the selective separation and preconcentration of U(VI).

1. Introduction

Uranium waste associated with several human activities, such as mining, nuclear fuel reprocessing in the nuclear industries, and so on, has high toxicity due to its long half-life and radioactive radiation.[1,2] The inhalation of uranium or uranium compounds may lead to progressive or irreversible renal injury, and in acute cases may result in kidney failure and death.[3] With better awareness of the healthy problems, the removal of trace amounts of uranium is essential for environmental cleanup, and the uranium recovered can also be used for nuclear fuel to reduce the energy consumption. These can be achieved through the strategy of imprinting.[4-6]

In the recent decades, the ion-imprinting technique was recognized as a convenient and powerful method for synthesizing specific recognition polymers by co-polymerizing functional and cross-linking monomers in the presence of desired template ions.[7-9] The ion-imprinted polymers have excellent memory effect and high selectivity to the imprinted ions. Most of the traditional ion-imprinted polymers prepared by the bulk polymerization exhibit high selective recognition but poor binding sites accessibility to the target ions, as the binding sites are totally situated deep inside the bulk of the polymer matrix which makes the mass transfer very low.[10] In order to overcome this problem, the surface ion-imprinted technique has attracted a lot of attentions, because the sites situated at the surface or in the proximity of materials surface not only enable the complete removal of templates, but also offer good accessibility to the target species and low mass-transfer resistance.[11,12] Up to now, there were a few reports on ion surface imprinting techniques.[13,14] Although the surface ion-imprinted polymers had selective sorption, they could not be separated rapidly and effectively from wastewater after treatment.[5,15] If the surface ion-imprinted polymers encapsulating Fe_3O_4 as nuclear can be synthesized, the materials with magnetic properties will be easily separated from aqueous solution using a magnetic field when compared to the centrifugation and filtration process.[16] Sadeghi and Aboobakri synthesized ferromagnetic nanoparticles with 3-aminopropyl triethoxysilane ligand for uranyl and its maximum sorption capacity was 8.2 $mg \cdot g^{-1}$.[17] Zhou et al.[18] reported that the monolayer sorption capacity of the ion-imprinted magnetic chitosan resins for U(VI) was 187.26 $mg \cdot g^{-1}$. These ion-imprinted composite sorption capacities were not high, and therefore uranyl ion-imprinted composites with higher maximum sorption capability and better selective sorption and reusability stability need to be further developed.

In this work, the U(VI) magnetic ion-imprinted composite (MIIC) was synthesized by sol-gel method and followed by copolymerization of a ternary complex of uranyl ions with 4-vinylpyridine (4-VP) and acrylamide in the presence of 2,2′-azobisisobutyronitrile (AIBN). Then the MIIC was characterized by scanning and transmission electron microscopy (SEM and TEM), powder X-ray diffraction (XRD), Fourier transform infrared (FT-IR) spectroscopy, and X-ray photoelectron spectroscopy (XPS) measurements. The sorption of U(VI) on MIIC from aqueous solutions was investigated by batch experiments.

2. Experimental Details

2.1. Materials. All the reagents were of analytical reagent grade and used as received. Milli-Q water was used in all experiments.

2.2. Preparation of Fe_3O_4 microspheres. Fe_3O_4 microspheres were synthesized by a hydrothermal method,[19,20] as follows: 1.35

g $FeCl_3 \cdot 6H_2O$ was dissolved in 75 mL glycol with magnetic stirring until it turned into transparent. Then 3.6 g sodium acetate was added and stirred vigorously for 10 min until the mixture became homogeneous, and then transferred into 100 mL Teflon-lined stainless steel autoclave at 200 °C for 16 h. After cooling to room temperature naturally, the precipitated products were centrifuged, and washed with ethanol and Milli-Q water for several times, and finally dried at 60 °C in an oven overnight.

2.3. Preparation of Fe_3O_4/SiO_2 microspheres. The prepared Fe_3O_4 magnetic microspheres were coated with a thin SiO_2 film (Fe_3O_4/SiO_2) using sol-gel method.[21] A certain amount of Fe_3O_4 microspheres were dispersed in the mixture of 2-propyl alcohol and Milli-Q water by sonication for 20 min. The mixture was continuously stirred, and followed by the addition of 5.0 mL ammoniumhydroxide (25wt%) and 2.0 mL tetraethyl orthosilicate (TEOS), and then kept stirring for 2 h. After that, the resultant product was collected by a magnet and washed with Milli-Q water to neutral. Finally, the Fe_3O_4/SiO_2 microspheres were dried under vacuum at 45 °C for 24 h.

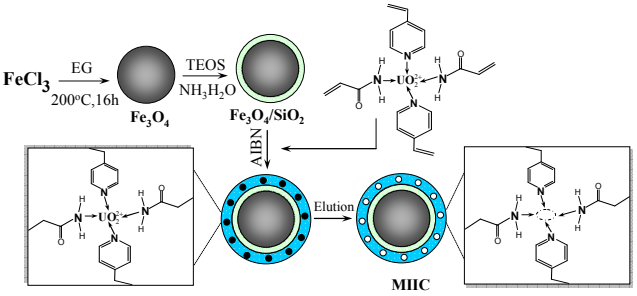

Figure 1. Schematic illustration of the synthesis route of MIIC.

2.4. Preparation of magnetic ion-imprinted composite. The synthesis of surface U(VI) ion-imprinted microspheres was carried out by thermal polymerization with the optimal synthesis conditions: 4-VP, acrylamide and ethylene glycol dimethacrylate (EGDMA) were applied as the functional monomers and cross linking agent respectively in the ratio of 1:2:2:20 (UO_2^{2+}: 4-VP: acrylamide: EGDMA) with AIBN as an initiator and 2-methoxyethanol as a porogen. The schematic illustration of the synthesis route of MIIC is shown in Figure 1. The ligands, which have the functional groups of $-NH_2$ or -C=N-, have strong complexing or chelating ability with uranyl ions. After the organic polymerization, the complexing coordination modes are retained. The ion-imprinted polymer with the special ligands can quickly recognize and selectively sorb the uranyl ions when they appear in the solutions. We simply propose the hypothesis as shown in Figure 1, but the actual complexing forms are more complex than we propose. The pre-polymerization mixtures were ultrasonicated for 20 min, cooled to 0 °C and then purged with N_2. Then, Fe_3O_4/SiO_2 microspheres were added with continuous stirring for 10 min and the polymerization was conducted in an oil bath at 60 °C while stirred for 1 h. After that, the obtained product was separated by an external magnet and washed with ethanol to remove all impurities. Finally, the template U(VI) ions were removed from the product (MIIC) by using 0.5 M HNO_3. The procedure was repeated several times until the template ions could not be detected in the filtrate. The obtained product was added into 0.1 M NaOH aqueous solution for 5–8 h to active amino group and then dried on vacuum oven for 8 h. Magnetic non-imprinted composite (MNIC) was similarly prepared without U(VI) ions by using the same synthetic procedure.

2.5. Characterization. The field emission SEM images were obtained with a JEOL JSM-6330F. The powder XRD were measured on a (Philips X'Pert Pro Super X-ray) diffractometer with a Cu Ka source (λ = 1.541 Å). FT-IR measurements were mounted by using a Perkin-Elmer 100 spectrometer over a range from 400 to 4000 cm^{-1}. The XPS measurements were conducted with a VG Scientific ESCALAB Mark II system. Magnetic measurements were performed in a vibrating sample magnetometer (VSM) with an applied magnetic field of 20 kOe.

2.6. Batch sorption experiments. Analytical-grade uranyl nitrate was employed to prepare a U(VI) stock solution. All sorption experiments were carried out using batch technique in a serial of 10 mL polyethylene test tubes. For U(VI) sorption, stock suspensions of MIIC, $NaNO_3$ and U(VI) were added in the test tubes, and the difference in the total volume of the mixtures was compensated by Milli-Q water to achieve the desired concentrations of different components. The pH values of the suspensions were adjusted by adding negligible volumes of 0.01 mol·L^{-1} HNO_3 or NaOH solutions. After the suspensions were shaken for 24 h, the solid phase was separated from the solution by using a conventional magnet. The concentrations of U(VI) in the filtrate were determined spectrophotometrically using Arsenazo III reagent.[17] The amount of U(VI) sorbed on MIIC was calculated from the followed equation.

$$q_e = \frac{(C_o - C_e)\cdot V}{m} \qquad (1)$$

where C_o is the initial concentration (mg·L^{-1}), C_e is the equilibrium concentration (mg·L^{-1}), q_e is the amount of U(VI) sorbed on the MIIC at equilibrium time (mg·g^{-1}), V is the solution volume (L), and m is the mass of the sorbent (g).

3. Results and Discussion

3.1. Characterizations of samples.

The SEM images of Fe_3O_4, Fe_3O_4/SiO_2, the magnetic ion-imprinted composite with U(VI) ions preserved on (U(VI)-MIIC), MIIC and MNIC are shown in Figure 2. Figure 2A shows that the Fe_3O_4 particles have approximately diameter of ~300 nm, and the surfaces relatively rough and uneven. After being coated with a nonporous silica layer, the core-shell Fe_3O_4/SiO_2 microspheres show smooth surfaces and uniform diameter on a large scale (Figure 2B). And after the copolymerization reaction with U(VI) ions, it can been seen from U(VI)-MIIC (Figure 2C) and MIIC (Figure 2D) that the flocculation-like co-polymers are evenly distributed on the Fe_3O_4/SiO_2 surfaces. However, the co-polymer (illustrated in Figure 2E) polymerized without U(VI) ions aggregates to a certain extent on the surfaces of Fe_3O_4/SiO_2 microspheres. Furthermore, the energy-dispersive X-ray spectroscopy (EDS) of U(VI)-MIIC shown in Figure 2F reveals the existence of C, O, Fe, Si and U elements, while Cu element results from the copper grids. And quantitative analysis shows that the mean atomic ratio (Si : O : U) in U(VI)-MIIC is 0.588 : 0.403 : 0.0013. To confirm the distributed composition of MIIC with U(VI) on the surface, TEM and the elemental map examinations are shown in Figure 3. The elemental map results

indicate that Si and O atoms are uniformly distributed, while the U is distributed on the surfaces of U(VI)-MIIC.

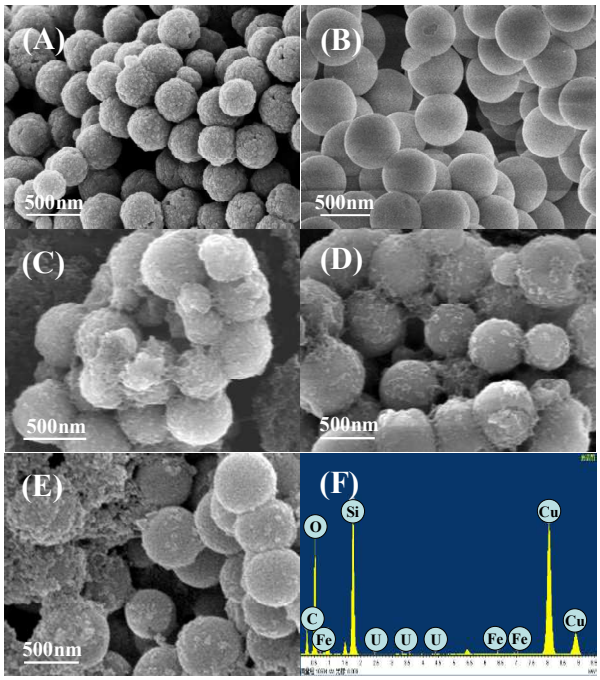

Figure 2. SEM images of Fe_3O_4 (A), Fe_3O_4/SiO_2 (B), U(VI)-MIIC (C), MIIC (D), MNIC (E) and EDS of U(VI)-MIIC.

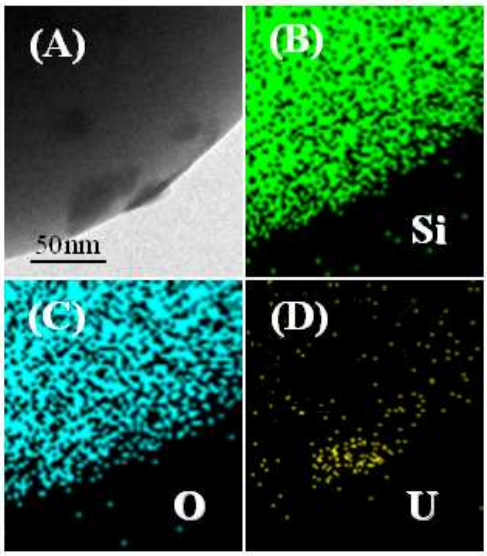

Figure 3. TEM of MIIC with U(VI) on the surface (A), elemental mapping of Si (B), O (C) and U (D).

Figure 4A shows XRD patterns of Fe_3O_4/SiO_2, U(VI)-MIIC, MIIC and MNIC. XRD patterns of Fe_3O_4/SiO_2 with six diffraction peaks for Fe_3O_4 can be indexed to (1 1 1), (2 2 0), (3 1 1), (4 0 0), (4 2 2), (5 1 1) and (4 4 0) (JCPDS Card No. 19-629) file.[22] It can also be seen that that the silica shell is amorphous, as evident from the presence of a broader hump at 20~25°. Compared with the spectrum of Fe_3O_4/SiO_2, the positions of all the characteristic diffraction peaks are unchanged upon U(VI)-MIIC, MIIC and MNIC. But, the intensity of the peaks slightly decreases, which confirms that the ion-imprinted composite is copolymerized on the surfaces of Fe_3O_4/SiO_2 microspheres.

Figure 4B shows FT-IR of all samples. The samples show sharp and strong peaks of Fe_3O_4 particles at 576 cm^{-1} and characteristic peaks of SiO_2 at 1102, 819, 961 and 465 cm^{-1}. The hydroxyl vibration peaks at 1633 and 3435 cm^{-1} reflect the presence of adsorption water. Compared with Fe_3O_4/SiO_2, the FT-IR spectra of U(VI)-MIIC, MIIC and MNIC reveal some new peaks as follows: at 1394 and 1465 (stretching C=C bond of pyridine ring), 1562 (the stretching and bending vibrations of -NH_2 groups), 1602 (C=N stretch of pyridine ring), 1725 (C=O stretching vibrations) and 2955 cm^{-1} (stretching vibrations of C–H bond).[23] The characteristic peak of UO_2^{2+} has been clearly observed at 836 cm^{-1} in U(VI)-MIIC, which is not appeared in the spectrum of MIIC. The result indicates that the U(VI) ions has been eluted from the magnetic ion-imprinted composite. From Figure 4B, it can also be seen that the magnetic eluted imprinted and non-imprinted composite show very similar location and appearance of the major bands.

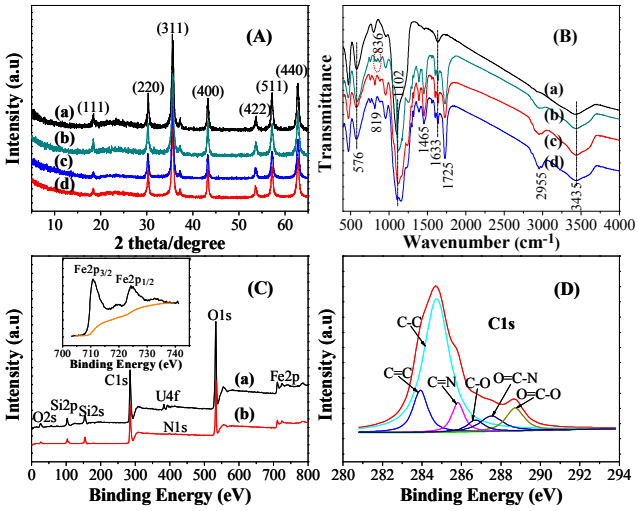

Figure 4. (A) XRD patterns of Fe_3O_4/SiO_2 (a), U(VI)-MIIC (b), MIIC (c) and MNIC (d), (B) FT-IR spectra of Fe_3O_4/SiO_2 (a), U(VI)-MIIC (b), MIIC (c) and MNIC (d), (C) XPS wide spectra of U(VI)-MIIC (a) and MIIC (b), and XPS spectrum of C1s of MIIC.

In order to concretely study the composition of magnetic core–shell structured materials, the XPS of U(VI)-MIIC and MIIC is measured. From Figure 4C, the peaks of Si2p (104.2 eV) and Si2s (155.8 eV) can be seen on two samples, which come from the silica coating. Compared with the spectrum of U(VI)-MIIC, the absence of the characteristic peak of U4f at around 390 eV in MIIC suggests the elution of U(VI) ions from the MIIC. The inset of Figure 4C shows that the binding energy of $Fe2p_{3/2}$ and $Fe2p_{1/2}$ are at 711.25eV and 724.78eV, respectively, which are consistent with the values of Fe_3O_4 reported in the literature.[24] Additionally, the C1s core-level spectrum of MIIC as shown in Figure 4D can be curve-fitted with five peak components with binding energies at 283.9, 284.6, 285.6, 286.5, 287.6, and 289.2 eV, attributed to C-C, C=C, C=N, C-O, C=O-N and O-C=O species, respectively.

The O-C=O specie in the C1s core-level spectrum may be resulted from polymerization during the cross-linking reaction with functional monomers on the surfaces of Fe_3O_4/SiO_2 microspheres.

The special saturation magnetization loops are shown in Figure 5. The saturation magnetizations, M_s, of Fe_3O_4/SiO_2 is 28.95 emu·g^{-1}. However, M_s of MIIC decreases to 25.94 emu·g^{-1}, which is mainly attributed to the existence of polymer on the surfaces of Fe_3O_4/SiO_2 microspheres. The left inset of Figure 5 indicates that the MIIC can be completely separated by placing a magnet near vessels. The magnetic separation of MIIC offers a simple and efficient route for separation and extraction of toxic metal ions from large volumes of aqueous solutions.

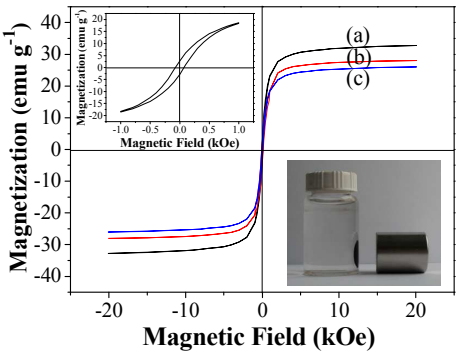

Figure 5. Magnetization curve of Fe_3O_4/SiO_2 (a), MNIC (b), and MIIC (c), the left inset is the magnified magnetization curve of MIIC and the below inset is the magnetic separation of MIIC.

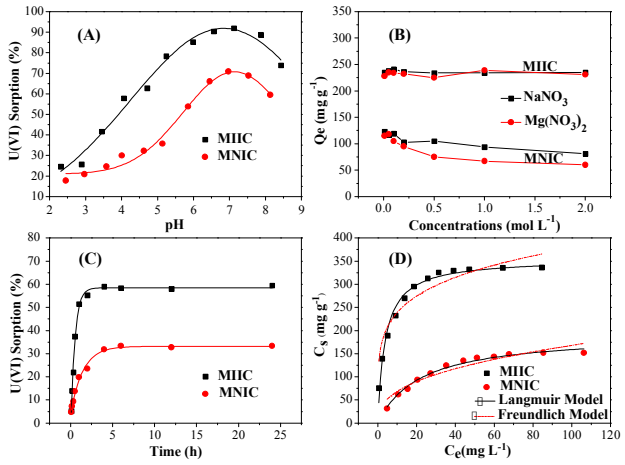

Figure 6. Different effects on the sorption of U(VI) onto MIIC and MNIC. (A) Effect of pH, at $C_{U(VI)initial}$ = 40.0 mg·L^{-1}, m/V = 0.1 g·L^{-1}, I = 0.01 M $NaNO_3$, and T = 293 K. (B) Effect of additional cations, at pH = 4.0 ± 0.1, $C_{U(VI)initial}$ = 40.0 mg·L^{-1}, m/V = 0.1 g·L^{-1}, and T = 293 K. (C) Effect of contact time, at pH = 4.0 ± 0.1, $C_{U(VI)initial}$ = 40.0 mg·L^{-1}, m/V = 0.1 g·L^{-1}, I = 0.01M $NaNO_3$, and T = 293 K, the black lines stand for the pseudo-second-order kinetic model and the red lines represent the pseudo-first-order kinetic model, (D) Sorption isotherms of U(VI), at pH = 4.0 ± 0.1, m/V = 0.1 g·L^{-1}, I = 0.01 M $NaNO_3$, and T = 293 K.

3.2. Different effects on U(VI) sorption. Figure 6A shows the sorption of U(VI) onto MIIC and MNIC as a function of pH. The sorption of U(VI) increases as the pH increases from 2.0 to 6.5. After that, the sorption of U(VI) reaches maximum at around pH 7.0, and follows by a reduce as the increase in pH. At an acidic medium, because the protonation of the amine moiety decreases the chelate ability of the amino groups with U(VI),[12] the sorption is low. Then the sorption increases with the weakened protonation as the pH increases. At higher pH values, the sorption efficiency decrease attributes to the formation of UO_2OH^+ and $(UO_2)_2(OH)_2$ as a result of the hydrolysis of U(VI) ions. Moreover, from Figure 6A, the MIIC exhibits a much higher sorption capacity for U(VI) than MNIC over the whole pH range. The reason may be due to that the interaction of U(VI) ions with amine moiety that randomly distributes all over the matrix of the composite without any structural arrangement substantially reduces the sorption efficiency.

Figure 6B shows the sorption of U(VI) on MIIC and MNIC as a function of ionic strength in different additional cation solutions. For MIIC, the equilibrium sorption capacities (q_e) in the $NaNO_3$ and $Mg(NO_3)_2$ solutions keep unchanged in general as the concentrations increase markedly. However, the sorption capacities of U(VI) on the MNIC decrease clearly. The orderly different sorption behavior certainly corresponds to different sorption mechanisms. No interference of additional cations on the sorption of U(VI) ions onto MIIC may be due to the identification and selectivity of the ion-imprinted composite to U(VI) ions. It is very important to extract and preconcentrate U(VI) from sea water which contains a large amount of cations (such as Na^+, Mg^{2+}, etc.).While for MNIC, higher ionic strength creates a higher shielding effect for U(VI) ions sorbed onto the MNIC surfaces, which causes a decrease in sorption. Additionally, outer-sphere surface complexes can also be considered to describe the decrease of U(VI) sorption on MNIC.

Figure 6C shows the sorption of U(VI) on MIIC and MNIC as a function of contact time. The sorption of U(VI) on MIIC is initially rapid and reaches equilibrium after approximately 90 min. Further increase in contact time do not show a significant increase in sorption. Compared with the sorption of U(VI) on MNIC, the sorption equilibrium of MIIC is much faster, which may be ascribed to that the rapid sorption at the first stage is not only owing to good affinity and strong chelation of imprinted cavities of MIIC toward U(VI), but also due to the smaller diffusion barrier in the thin imprinted composite layer for U(VI). The kinetic sorption of U(VI) on MIIC and MNIC is simulated with the pseudo-first-order and pseudo-second-order models. The linearized form of the pseudo-first order equation is generally expressed as equation 2.[25]

$$Log(q_e - q_t) = Logq_e - \frac{K_1}{2.303}t \qquad (2)$$

The pseudo-second-order equation is given as equation 3.[26]

$$\frac{t}{q_t} = \frac{1}{K_2 q_e^2} + \frac{t}{q_e} \qquad (3)$$

where q_t (mg·g^{-1}) is the amount of U(VI) sorbed on MIIC and MNIC at time t (h), q_e (mg·g^{-1}) is the equilibrium sorption capacity, K_1 (g·mg^{-1}·h^{-1}) is the pseudo-first-order rate constant of

sorption and K_2 (g·mg^{-1}·h^{-1}) is the pseudo-second-order rate constant of sorption.

Table 1. Constants for the kinetic sorption data using different sorption models.

models	pseudo-first-order		pseudo-second-order	
MIIC	q_e (mg·g^{-1})	245.7	q_e (mg·g^{-1})	242.3
	K_1 (h^{-1})	2.18	K_2 (g·mg^{-1}·h^{-1})	0.013
	R^2	0.958	R^2	0.999
MNIC	q_e (mg·g^{-1})	129.4	q_e (mg·g^{-1})	138.9
	K_1 (h^{-1})	0.919	K_2 (g·mg^{-1}·h^{-1})	0.011
	R^2	0.954	R^2	0.998

The parameters of two kinetic sorption models are listed in Table 1. From Table 1, it can be seen that the estimated q_e (242.3 mg·g^{-1}) value derivated from the pseudo-second-order kinetic model is much closer to the experimental q_e (237.8 mg·g^{-1}) value. The correlation coefficient of the pseudo-second-order kinetic model for the linear plots is much higher than that of the pseudo-first-order model. These results suggest that the sorption of U(VI) on MIIC was very well described by the pseudo-second-order model.

The maximum sorption capacity is one of the most important factors to quantitatively remove and concentrate U(VI). As shown in Figure 6D, with the increase of U(VI) concentrations, the sorption capacities first increase sharply, then increase slightly, and finally reach saturation. To gain a better understanding of sorption mechanisms and to quantify the sorption data, the Langmuir and Freundlich models are used to simulate the experimental data.

The Langmuir can be expressed by the following equation.

$$C_s = \frac{bC_{s\max}C_e}{1+bC_e} \qquad (4)$$

where C_{smax} (mg·g^{-1}) represents the maximum sorption capacity, and b (L·mg^{-1}) is the constant that relates to the heat of sorption.

The Freundlich model can be represented by the following equation.

$$C_s = K_F C_e^{\,n} \qquad (5)$$

where K_F (mol^{1-n}·L^n·g^{-1}) is the sorption capacity when metal ion equilibrium concentration equals to 1, and n represents the degree of dependence of sorption with equilibrium concentration.

Table 2. The parameters of the Langmuir and Freundlich models for the sorption isotherm.

Models	Langmuir			Freundlich		
Parameters	C_{smax} (mg·g^{-1})	b (L·mg^{-1})	R^2	k_F (mol^{1-n}·L^n·g^{-1})	n	R^2
MIIC	354.85	0.26	0.976	151.32	0.20	0.899
MNIC	168.27	0.08	0.986	27.9	0.39	0.906

From Table 2, the Langmuir model fits the experimental data better than the Freundlich model, and the maximum sorption capacities of U(VI) on MIIC (354.85 mg·g^{-1}) is much higher than that of MNIC (168.27 mg·g^{-1}). The reason is maybe due to the homogeneous distribution of cavities for the selective sorption of U(VI) on the surface of MIIC. Table 3 displays a comparison of the maximum sorption capacity of MIIC with that of other sorbents, indicating the excellent sorption abilities of MIIC toward U(VI).

In order to tested the selectivity of the MIIC, the competitive sorption experiments were investigated by preparing mixed solutions, in which the concentration of U(VI) was the same as other ions. The selective sorption properties of MIIC are evaluated by distribution coefficient (D), selectivity coefficient (K), and relative selectivity coefficient (K_r). The distribution coefficient was calculated from the equation.

$$D = \frac{Q_e}{C_e} \qquad (6)$$

where D is the distribution coefficient, and Q_e (mg·L^{-1}) is the equilibrium binding quantity. The selectivity coefficient for U(VI) sorption with competitor metal ions can be obtained from equilibrium binding data according to the following equation.[32]

$$K = \frac{D_{UO_2^{2+}}}{D_{M^{n+}}} \qquad (7)$$

where K is the selectivity coefficient and M^{n+} represents competitor metal ions. K represents U(VI) sorption selectivity when other metal ions coexist in the solution. A relative selectivity coefficient, K_r could be expressed as follows.[32]

$$K_r = \frac{D_i}{D_n} \qquad (8)$$

where K_i and K_n represent the selectivity coefficients of the MIIC and MNIC, respectively. K_r is the difference of metal ion sorption affinity recognition of sites to the imprinted U(VI) between them.

Table 3. The comparison of the maximum sorption capacity (C_{smax}) of MIIC with that of other sorbents.

Adsorbents	pH	C_{smax} (mg·g^{-1})	Reference
Multi-walled carbon nanotubes	5.0	26.18	27
Oxime-grafted ordered mesoporous carbon CMK-5	4.5	65.18	28
Cross-linked chitosan	3.0	72.46	29
Graphene oxide nanosheets	5.0	97.5	30
Ion-imprinted chitosan/PVA cross-linked hydrogel	5.0	156	31
Ferromagnetic nanoparticles with an imprinted polymer	4.0	8.2	17
Ion-imprinted magnetic chitosan resins	5.0	187.26	18
Magnetic non-imprinted composite	4.0	168.27	This work
Magnetic ion-imprinted composite	4.0	354.85	

The selective sorption parameters of MIIC with respect to other metal ions are shown in Table 4. The distribution coefficient of MIIC for U(VI) is 5.3 times than that of MNIC. Furthermore, the relative selectivity coefficient of MIIC for each

individual metal ion is much higher than 1. These observations are ascribed to the specific recognition cavities for U(VI) created in MIIC, developed by ion imprinting on the surfaces of MIIC. MIIC has a strong ability to selectively sorb U(VI) from other metal ions coexisting in the aqueous solutions.

Table 4. Selective sorption of U(VI) on MIIC and MNIC ($C_{U(VI)initial}$ = 40.0 mg·L^{-1}, m/V = 0.1 g·L^{-1}, pH = 4.0 ± 0.1, T = 298 K).

Metal ions	MIIC		MNIC		*K*r
	D	*K*	*D*	*K*	
U(VI)	14384		2698		
Cr(VI)	3158	4.55	2422	1.11	4.10
Cu(II)	1799	8.00	1396	1.93	4.15
Eu(III)	1001	14.38	647	4.17	3.45
Ni(II)	455	31.61	341	7.91	4.01
Cd(II)	291	49.40	270	9.99	4.94
Co(II)	233	61.70	186	14.50	4.26

Table 5. Five cycles of the U(VI) sorption/desorption with 0.5 mol·L^{-1} HNO_3 solution as the desorbing agent. Initial concentration of U(VI) =120 mg·L^{-1}, pH = 4.0 ± 0.1, and T = 293 K.

Cycle numbers	Sorption		Desorption (%)
	mg·g^{-1}	%	
1	350.23	98.34	96.7
2	344.15	96.6	95.8
3	343.67	96.50	95.6
4	358.54	100.67	94.3
5	347.22	97.49	94.4

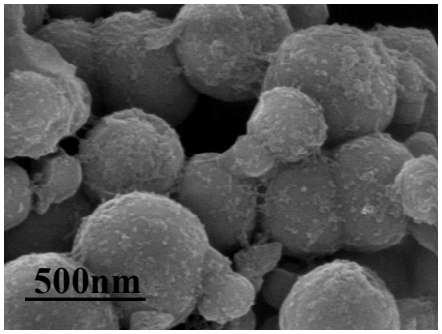

Figure 7. SEM image of MIIC after five consecutive sorption/desorption cycles.

In general, the ion-imprinted nanoparticle frame is highly dependent on the organic framework. These will be sensitive to solution or acidic pH which will make ion-imprinted composites fall apart or be unusable if they are used more than once. It also makes very little sense to have to template them around uranium to be able to recover or extract uranium. This is not very efficient and not likely to be cost effective in remediation of environmental contaminated sites. So the reusability of MIIC in the removal of U(VI) was confirmed by adopting 0.5 mol·L^{-1} HNO_3 as desorbing agent and the results are presented in Table 5. From Table 5, the sorption capacity of U(VI) decreases slightly from 350.23 mg·g^{-1} in the first cycle to 347.22 mg·g^{-1} in the fifth cycle, while the recovery of U(VI) ions sorbed from the surfaces of MIIC decreases from 96.7% to 94.4% after five consecutive sorption/desorption cycles. The results suggest that the MIIC can be efficiently regenerated by 0.5 mol·L^{-1} HNO_3 and reused with also high U(VI) sorption capability after 5 cycles. The surface morphology of MIIC after consecutive sorption/desorption cycles was also tested. From Figure 7, no obvious change in the morphology of MIIC is observed after 5 cycles. The sorbent that not only possesses higher sorption capability but also shows better desorption property will significantly reduce the overall cost for practical applications.

4. Conclusions

The magnetic ion-imprinted composite (MIIC) with a uniform core–shell structure was fabricated by sol-gel method and followed by copolymerization. The sorption of U(VI) on the MIIC from the aqueous solution was evaluated by batch experiments. The results suggest that the combination of the magnetic properties of Fe_3O_4 microspheres and the superior selective sorption properties of the ion-imprinted composite makes a powerful separation material for the selective separation and preconcentration of U(VI).

Acknowledgements

The National Natural Science Foundation of China (91126020, 41273134, 21107115, 91326202 and 21225730) was acknowledged.

Notes and references

Institute of Plasma Physics, Chinese Academy of Sciences, P.O. Box 1126, Hefei 230031, PR China. Fax: +86-551-65591310; Tel: +86-551-65593308; Email: clchen@ipp.ac.cn (C. L. Chen).

1 M.J. Monreal and P.L. Diaconescu, *Nat. Chem.*, 2010, **2**, 424.
2 S. Yan, B. Hua, Z. Bao, J. Yang, C. Liu and B. Deng, *Environ. Sci. Technol.*, 2010, **44**, 7783-7789.
3 C.R. Preetha, J.M. Gladis and T.P. Rao, *Environ. Sci. Technol.*, 2006, **40**, 3070-3074.
4 P. Metilda, J.M. Gladis and T.P. Rao, *Anal. Chim. Acta*, 2004, **512**, 63–73.
5 M. Shamsipur, J. Fasihi and K. Ashtari, *Anal. Chem.*, 2007, **79**, 7116–7123.
6 D. James, G. Venkateswaran and T.P. Rao, *Microporous Mesoporous Mater.*, **119**, 2009, 165-170.
7 Z. Zhang, S. Saengkerdsub and S. Dai, *Chem. Mater.,* 2003, **15**, 2921-2925.
8 H. Liu, F. Yang, Y. Zheng, J. Kang, J. Qu and J.P. Chen, *Water Res.*, 2011, **45**, 145-154.
9 M. Saraji and H. Yousefi, *J. Hazard. Mater.*, 2009, **167**, 1152–1157.
10 J. Pan, X. Zou, Y. Yan, X. Wang, W. Guan, J. Han and X. Wu, *Appl. Clay Sci.*, 2010, **50**, 260-265.
11 G. Fang, J. Tan and X. Yan, *Anal. Chem.*, 2005, **77**, 1734-1739.
12 Y. Zhan, X. Luo, S. Nie, Y. Huang, X. Tu and S. Luo, *Ind. Eng. Chem. Res.*, 2011, **50**, 6355–6361.
13 X. Bi, R. J. Lau and K. L. Yang, *Langmuir*, 2007, **23**, 8079-8086.
14 B. Gao, F. An and Y. Zhu, *Polymer*, 2007, **48**, 2288-2297.
15 S. J. Ahmadi, O. N. Kalkhoran and S. S. Arani, *J. Hazard. Mater.*, 2010, **175**, 193–197
16 Q.H. Fan, P. Li, Y.F. Chen and W.S. Wu, *J. Hazard. Mater.*, 2011, **192**, 1851-1859.
17 S. Sadeghi and E. Aboobakri, *Microchim. Acta*, 2012, **178**, 89–97.
18 L.M. Zhou, C. Shang, Z.R. Liu, G.L. Huang and A.A.A. Adesina, *J. Colloid Interface Sci.*, 2012, **366**, 165-172.

19 D. Qi, H. Zhang, J. Tang, C. Deng and X. Zhang, *J. Phys. Chem. C*, 2010, **114**, 9221–9226.

20 H. Deng, X. Li, Q. Peng, X. Wang, J. Chen and Y. Li, *Angew. Chem. Int. Ed.*, 2005, **117**, 2842–2845.

21 X. Wang, L. Wang, X. He, Y. Zhang and L. Chen, *Talanta*, 2009, **78**, 327-332.

22 W. Wang, Y. Zhang, Q. Yang, M. Sun, X. Fei, Y. Song, Y. Zhang and Y. Li, *Nanoscale*, 2013, **5**, 4958-4965.

23 T. E. Milja, K.P. Prathish and T.P. Rao, *J. Hazard. Mater.*, 2011, **188**, 384-390.

24 B.J. Tan, K. J. Klabunde and P.M.A. Sherwood, *Chem. Mater.*, 1990, **2**, 186-191.

25 Y. S. Ho and G. McKay, *Process Saf. Environ. Prot.*, 1998, ***76***, 332–340.

26 Y. S. Ho, and G. McKay, *Water Res.*, 2000, **34**, 735–742.

27 D. Shao, Z. Jiang, X. Wang, J. Li and Y. Meng, *J. Phys. Chem. B*, 2009, **113**, 860–864.

28 G. Tian, J. Geng, Y. Jin, C. Wang, S. Li, Z. Chen, H. Wang, Y. Zhao and S. Li, *J. Hazard. Mater.*, 2011, **190**, 442–450.

29 G. Wang, J. Liu, X. Wang, Z. Xie and N. Deng, *J. Hazard. Mater.*, 2009, **168**, 1053–1058.

30 G. Zhao, T. Wen, X.Yang, S. Yang, J. Liao, J. Hu, D. Shao and X. Wang, *Dalton Trans.*, 2012, **41**, 6182–6188.

31 Y. Liu, X. Cao, R. Hua, Y. Wang, Y. Liu, C. Pang and Y. Wang, *Hydrometallurgy*, 2010, **104**, 150–155.

32 E. Birlik, A. Ersoz, E. Acıkkalp, A. Denizli and R. Say, *J. Hazard. Mater.*, 2007, **140**, 110–116.

GRAPHICAL ABSTRACT

The synthesis route of magnetic ion-imprinted composite